Improved Low-Cost GNSS-R Altimetry by Recursive Temporal Continuity Constraints

Kaoru Ichikawa[1], Takuji Ebinuma[2], and Chuan Bing Wang[3]

[1]Research Institute for Applied Mechanics, Kyushu University, 6-1 Kasuga-kouen, Kasuga, Fukuoka 816-8580, Japan.

[2]College of Engineering, Chubu University, Kasugai 487-8501, Japan.

[3]Department of Earth System Science and Technology, Kyushu University, 6-1 Kasuga-kouen, Kasuga, Fukuoka 816-8580.

Corresponding author: Kaoru Ichikawa (ichikawa@riam.kyushu-u.ac.jp)

Key Points:

- A low-cost altimeter to measure water levels of lakes or coastal seas has been achieved by two classical GNSS receivers on a small UAV
- The accuracy is improved by recursive constraints of temporal continuity, suppressing large high-frequency variations
- The accuracy depends on elevation angles of GNSS satellites, and also is sensitive to contaminations of unexpected reflections from lands

Abstract

Global Navigation Satellite System (GNSS) signals reflected at the water surface are received together with direct GNSS signals by two low-const receivers deployed to an unmanned aerial vehicle (UAV). From relative delay of the reflected signals with respect to the direct ones, the height of the UAV above the water surface can be determined by GNSS Reflectometry (GNSS-R). The height estimation is originally conducted independently for each epoch, but by forcing temporally continuous constraints on differences of two receiver clocks, estimates of whole epochs during the study period are then contributed in the recursive estimates of the height. Applying the new method to GNSS-R altimetry data during an approximately 3-min hovering period at around 120-m altitude, the mean and RMS differences from the measured and estimated heights become improved from 0.72 and 5.87 m to 0.35 and 3.74 m. The accuracy of measurements is also found strongly depends on elevation angles of GNSS satellites, and also is sensitive to contaminations of unexpected reflections such as from lands or ships.

Plain Language Summary

Recently, a low-cost altimeter mounted on an unmanned aerial vehicle (UAV) has been developed, which enables to measure water surface height at any time and location. Since Global Navigation Satellite System (GNSS) signals reflected at the water surface and received at the UAV always travel longer than the signals directly received at the UAV, the excess path length of the reflected GNSS signals is used to estimate the height of the UAV above the water surface. These estimations were conducted independently at each 5-Hz sampled observation time, but the new method proposed in the present study forces to contribute whole observations during the study period in estimations at each observation time, assuming that clock precision of the GNSS receivers does not change abruptly. The accuracy of the height estimation has been improved to reduce 50% of estimation errors.

1 Introduction

Measurements of water surface height are one of the most fundamental research activities for disaster preventions (e.g. tsunami and flood), monitoring water mass volumes (e.g., rivers, lakes, points and global oceans) and also researches of oceanic variations (e.g. waves, tides and geostrophic velocities). Satellite altimeters have provided unique observations of the sea surface height in open oceans (e.g. Fu and Cazenave, 2001), but their use in coastal areas is limited since an conventional altimeters' assumption of homogeneous reflections of microwaves within footprints often corrupts in coastal areas (e.g. Passaro et al., 2014; Ichikawa et al., 2020). Instead, various types of water level gauges are available at fixed positions along coastlines or lakesides.

Nevertheless, more frequent and/or dense observations of water surface would be necessary since temporal and spatial variations in coastal areas, lakes or ponds are generally small. Moreover, some fixed gauge stations may not be in operation in cases of disasters. Therefore, a method is required to measure water levels at an arbitrary time and place. Note that this method would be also useful to calibrate new wide-swath altimeters, such as SWOT (Surface Water and Ocean Topography) mission (Fu et al., 2017).

Global Navigation Satellite System (GNSS) is one of most practical solutions to determine water surface height at an arbitrary time and place. GNSS receivers deployed on surface drifters or mooring systems can directly measure water level, although difficulty of their deployment and recovery may limit periods and locations of measurements. Meanwhile, significant mobility of measurements would be expected for shipborne and airborne altimeters (e.g. Cretaux et al., 2011) . These altimeters consist of two measurements; precise height estimations of GNSS receivers on the ships or aircrafts and additional measurements of vertical distance between the GNSS receivers and the water surface beneath.

Light Detection And Ranging (LiDAR) altimetry (e.g., Zlinszky et al., 2017; Lin et al., 2019; Fayad et al., 2020) is often used in airborne altimeters to measure the distance from the water surface. It can accurately measure a range between the LiDAR sensor and the reflection points on the water surface, but since its nadir footprint is narrow, accuracy of the range measurements would be sensitive to the attitude of the LiDAR sensor, slope of the water surface caused by waves, or presence of floating materials on the water surface.

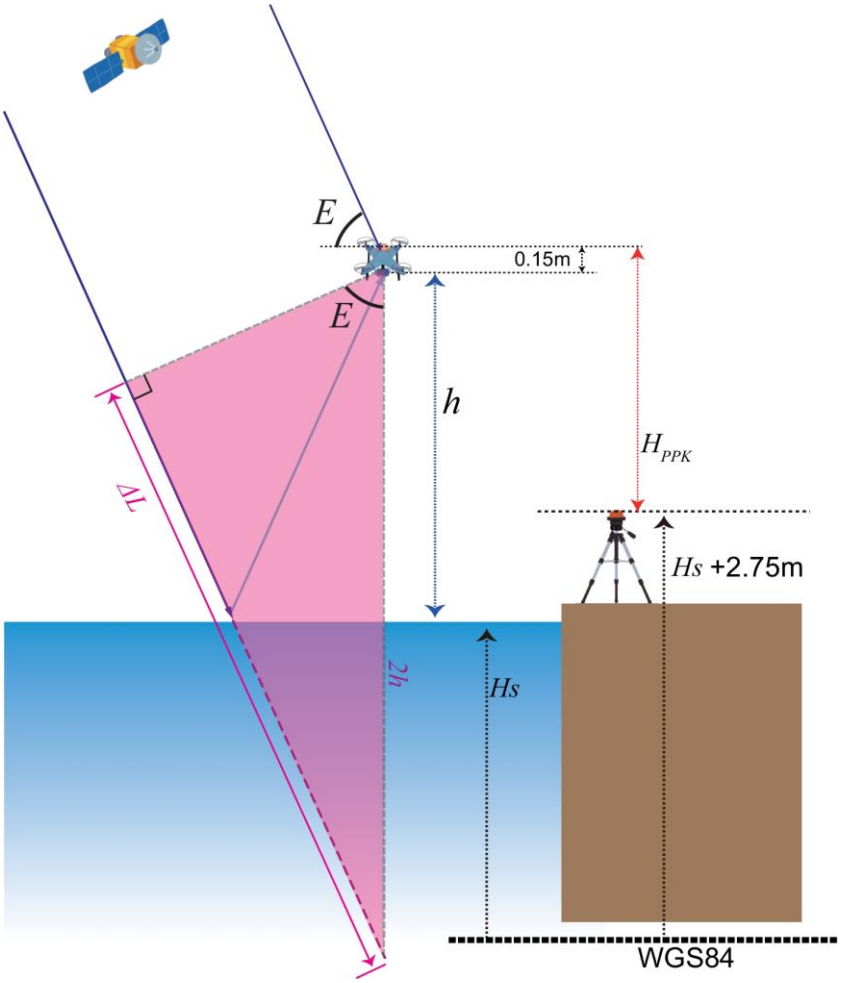

Figure 1. Schematic figure of GNSS-R altimetry in Ichikawa et al. (2019). The height of a UAV with respect to the water level, h, was measured by the PPK positioning method referring to an in situ base station. Meanwhile, h was estimated from simultaneous observations of the delays, ΔL_i, of reflected signals of GNSS satellites whose elevation angles are E_i $(i = 1, 2, \dots, N)$.

GNSS Reflectometry (GNSS-R) is another solution to obtain vertical distance between the water surface and ships or aircrafts. As shown in Fig.1, the path length of GNSS signals reflected at water surface is always longer than that of the direct GNSS signals. Therefore, from the temporal delay of the reflected signals with respect to the direct signals, vertical distance of the water surface and the receiver, *h*, can be obtained (e.g., Lowe et al., 2002; Martin-Neira et al., 2002; Ruffini et al., 2004; Roussel et al., 2014). In order to accurately obtain the temporal delay, the direct and reflected GNSS signals should be recorded by synchronized receivers, otherwise floating clock difference between the two receivers will be included as an unknown error.

Recently, Ichikawa et al. (2019) has reported a low-cost GNSS-R altimeter that uses two independent classical receivers on a small unmanned aerial vehicle (UAV); generally, synchronized receivers are significantly expensive than classical receivers. Since signals of all GNSS satellites are recorded at the same time, the difference of the clocks of two receivers are common for all GNSS satellites at a given epoch. Therefore, the clock difference can be solved for each epoch by the least square method applied to signals of several GNSS satellites. Their method has achieved 0.03-m accuracy in observing the water level of a lake, although which strongly depends on the number of available GNSS satellites and the altitude of the UAV; with the smaller number of available GNSS satellites and the higher UAV altitude, the worse the accuracy becomes. In addition, the estimated height *h* includes significantly large high-frequency fluctuations, reaching the root mean squared (rms) difference exceeding 3 m even at the best estimates.

In the present study, we further extend the method in Ichikawa et al. (2019) to force temporally continuity of independent estimations at each single epoch. The clock accuracy of a receiver may be influenced by environmental factors such as mechanical vibrations, temperature and pressure, but its variation should be temporally gradual under calm environmental changes. Based on this assumption, we constrain gradual temporal changes of the floating clock differences that have been estimated independently for each epoch. The modified method will be applied in this study to the data during the period when the UAV was hovering at a high altitude, namely the worst estimates in the Ichikawa et al. (2019). The materials and methods used in this study are explained in Section 2, followed by descriptions of the results in Section 3. Discussion and summary are described in Section 4.

2 Materials and Methods

Ichikawa et al. (2019) made experimental flights at the western coast of Lake Biwa (35.319°N, 136.077°E), Japan on 7 January 2017, during the period 12:00–14:00 JST. Two antennas (Tallysman TW4721 and Antcom 4G15L-A-XS-1) were mounted on a quadcopter (DJI Phantom 2 Vision+) to receive the direct and reflected GNSS signals, respectively. These were recorded at the 5 Hz rate by two independent classical receivers (ublox NEO-M8T). Due to the limitation of the antennas, only Global Positioning System (GPS) L1 band signals were used. In addition, since all flights were conducted at the lakeside, signals of GPS satellites located to the west of the UAV were eliminated since their reflection points could be on lands rather than on the water surface.

A geodetic 1-Hz GNSS receiver (Hitz NetServe RE) was additionally deployed as an in situ base station, whose height was 2.75 m above the water level *Hs*. The vertical height of the UAV, H_{PPK}, was estimated using the post-processed kinematic (PPK) positioning method (RTKLIB, 2018). Since the antenna receiving reflected GNSS signals was deployed 0.15 m

below the other antenna for the direct GNSS signals, its measured height above the water level, *Ha*, is determined as $Ha = H_{PPK}$ +2.75 -0.15 m (Fig. 1).

For a given GNSS satellite with the elevation angle E_i, (Fig. 1), the path length of the reflected GNSS signal is longer than the direct GNSS signal by $2h\sin Ei$, where h is the height of the antenna on the UAV (Fig. 1). Meanwhile, the observed delay ΔL_i would be affected by an unknown floating clock difference between two receivers, ΔT. Since all GNSS satellites are observed at the same time, the clock difference is common for all GNSS satellites. Therefore, from $i = 1, 2, \ldots, N$ satellite observations at an epoch, the following simultaneous equations can be formulated.

$$\begin{bmatrix} \Delta L_1 \\ \vdots \\ \Delta L_N \end{bmatrix} = \begin{bmatrix} 2\sin(E_1) & 1 \\ \vdots & \vdots \\ 2\sin(E_N) & 1 \end{bmatrix} \begin{bmatrix} h \\ c\Delta T \end{bmatrix} + \begin{bmatrix} \epsilon_1 \\ \vdots \\ \epsilon_N \end{bmatrix}, \quad (1)$$

where c is the speed of light and ϵ_i is an observational noise. Using the least square method, the height h and the clock differences ΔT can be estimated simultaneously as in the following equation,

$$\begin{bmatrix} \sum \Delta L_i \sin(E_i) \\ \sum \Delta L_i \end{bmatrix} \sim \begin{bmatrix} 2\sum \sin^2(E_i) & \sum \sin(E_i) \\ 2\sum \sin(E_i) & \sum 1 \end{bmatrix} \begin{bmatrix} h \\ c\Delta T \end{bmatrix}. \quad (2)$$

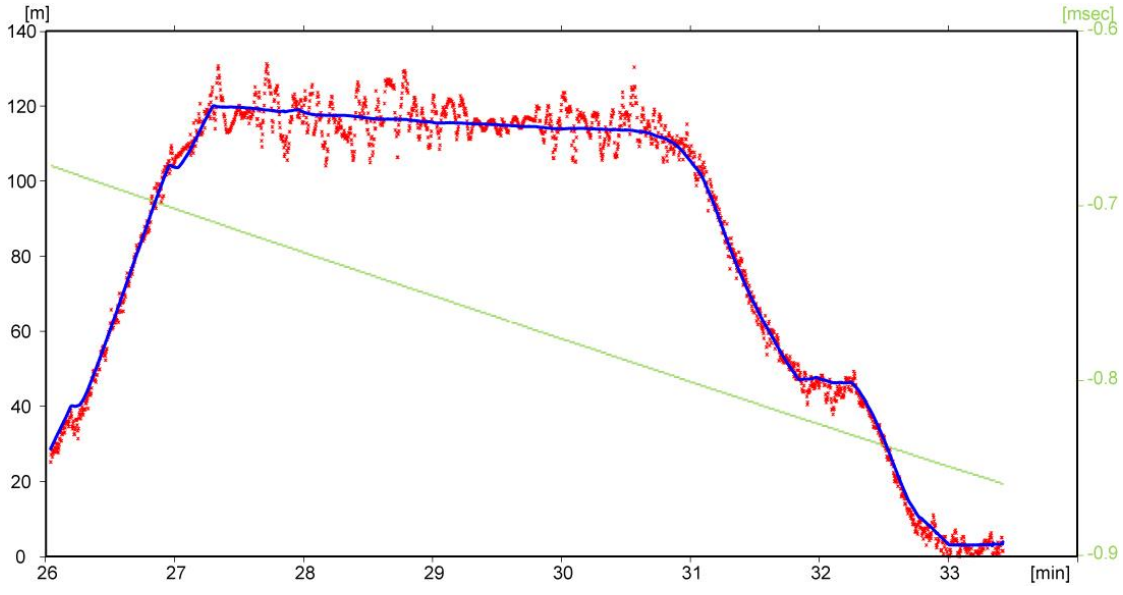

Figure 2. Time series of the estimated height *h* (red) and measured height *Ha* (blue) (left ordinate) at one of the flights in Ichikawa et al. (2019). The simultaneously estimated ΔT is also plotted by greed dots (right ordinate). The abscissa is the elapsed time in minutes from noon on 7 January 2017 (JST).

Figure 2 shows an example of results in Ichikawa et al. (2019). The UAV moved straight upward and hovered for nearly four minutes at an approximately 120-m altitude, then moved downward. The estimated height *h* clearly followed the measured height *Ha*, although high-frequency fluctuations whose amplitudes are larger than 10 m are included during the hovering period (from 27.5 to 31 min). Meanwhile, the simultaneously estimated floating

clock difference ΔT showed constant gradual changes, independently from the altitude of UAV.

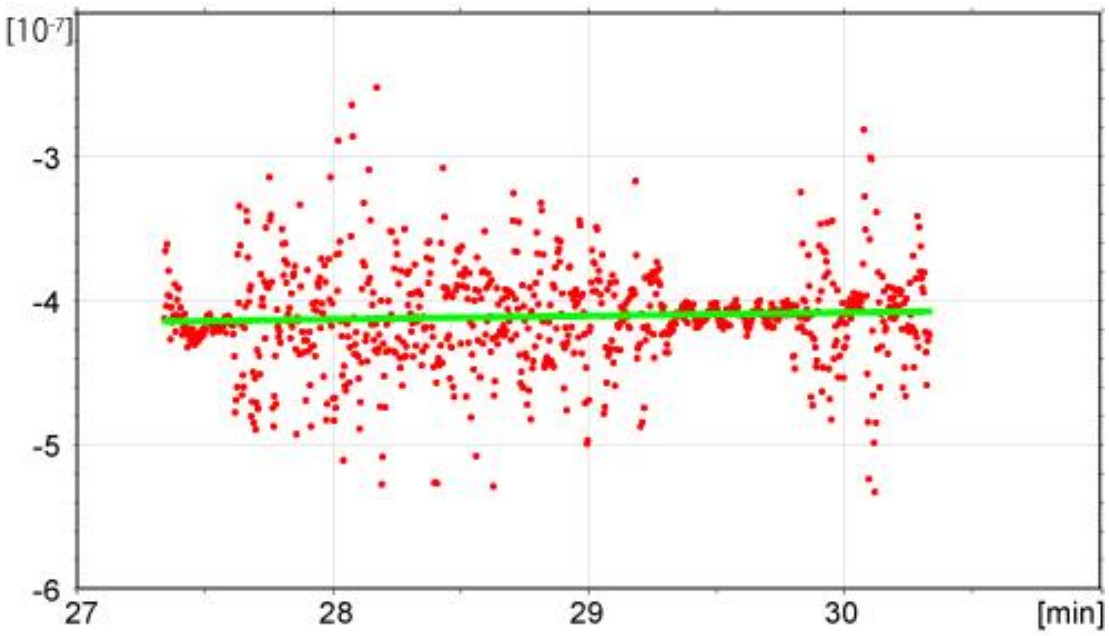

Figure 3. Temporal change rate of the estimated floating clock difference ΔT shown in Fig. 2 (red dots) and that of the quadratic-fitted ΔT^e (green dots) estimated by the least square method applied to ΔT.

However, the temporal change rate of ΔT was not actually constant. The change rate $d(\Delta T)/dt$ during the hovering period (when the vertical speed of the UAV, dH_a/dt, was within ± 0.1 ms^{-1}) at approximately 120 m altitude indicates that it also includes high-frequency fluctuations around the mean value (Fig. 3). Since ΔT is mainly caused by difference of clock accuracy of the receivers, which should not change abruptly with the steady environmental conditions during the hovering, these high-frequency fluctuations of the estimated ΔT would not be real changes but errors of the ΔT estimations associated with wrong estimations of h that is simultaneously determined . Therefore, temporally-gradual ΔT^e determined by the quadratic-fit of ΔT is introduced to eliminate these high-frequency noises (Fig. 3). By subtracting ΔT^e in Eq. (1), the simultaneous equations becomes

$$\begin{bmatrix} \Delta L^e{}_1 \\ \vdots \\ \Delta L^e{}_N \end{bmatrix} = \begin{bmatrix} \Delta L_1 - c\Delta T^e \\ \vdots \\ \Delta L_N - c\Delta T^e \end{bmatrix} = h \begin{bmatrix} 2\sin(E_1) \\ \vdots \\ 2\sin(E_N) \end{bmatrix} + \begin{bmatrix} \epsilon_1 \\ \vdots \\ \epsilon_N \end{bmatrix}. \quad (3)$$

Using the least square method, the height h can be estimated from $\Delta L^e{}_i$ as in the following equation

$$\sum \Delta L^e{}_i \sin(E_i) \sim 2h \sum \sin^2(E_1). \quad (4)$$

Furthermore, if the observational noise ϵ_i is negligibly small, h can be roughly estimated from Eq. (3) by $\Delta L^e{}_i/2\sin(E_i)$ for each individual GNSS satellite.

3 Results

In this study, we choose the worst accuracy case when the UAV was hovering at a high altitude (approximately 120 m) in the first flight of Ichikawa et al. (2019). Five GNSS satellites were available during this study period (Table 1). Since the sampling rate was 5 Hz, 895 epochs are used during the 179-second period, except for one GPS satellite whose pseudo random noise (PRN) number is 44. Most satellites were located to the northeast/east of the UAV, but the satellite with PRN 44 was located to the south of UAV. Since a shoal was extended to the south/southeast of the observation site, missing observations of PRN 44 could be affected by unexpected reflection from the lands.

Table 1. *GPS Satellites used in the Analysis*

PRN	Elevation angles [deg]	Azimuth angle [deg]	epochs
13	58.0 to 56.9	29.1 to 30.6	895
28	11.3 to 11.6	68.0 to 66.7	895
30	9.8 to 8.7	39.6 to 39.3	895
5	43.3 to 42.3	106.8 to 108.2	895
44	44.3 to 44.6	152.3 to 153.4	758

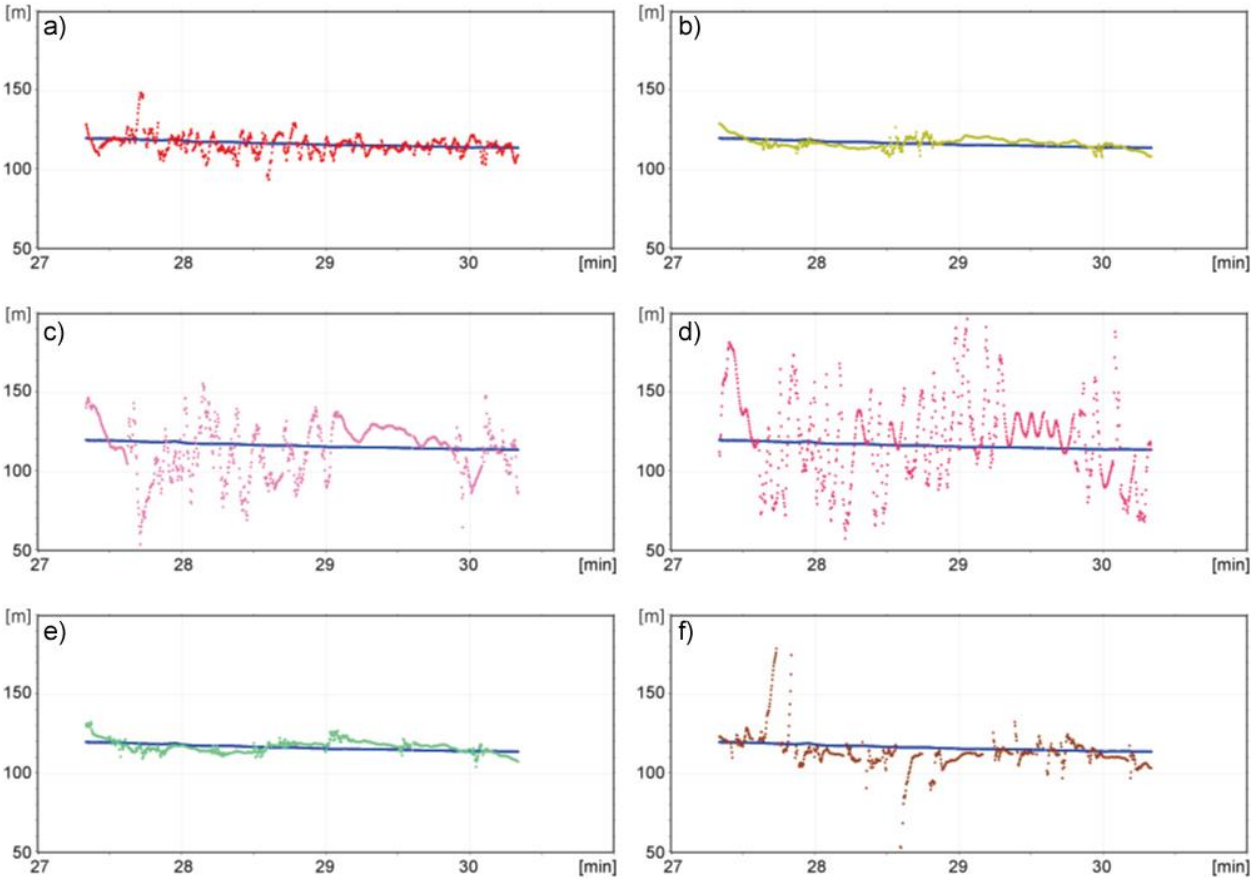

Figure 4. Time series of the original estimated height *h* as in Fig. 2 (**a**), and rough estimations of the height *h* by $\Delta L^e{}_i/2\sin(E_i)$ in Eq. (3) for PRN 13 (**b**), 28 (**c**), 30 (**d**), 5 (**e**) and 44 (**f**). The measured height *Ha* is plotted by blue dots in all panels for reference.

After subtracting the quadratic-fitted ΔT^e, the height *h* is roughly estimated for individual GPS satellites as $\Delta L^e{}_i/2\sin(E_i)$ in Eq. (3), assuming that the observational noise ϵ_i is small (Fig. 4). Comparing with the original estimation of the height *h* shown in Fig. 2 (Fig. 4a), two panels (Fig. 4b and 4e) show less fluctuations but the others exhibit extremely larger fluctuations. As shown in Table 2, the RMS difference from the measured height *Ha* for the original estimation (5.87 m) is larger than those for PRN 13 (3.30 m) and PRN 5 (3.82 m), but smaller than those for PRN 28, 30 and 44 (17.07, 26.80, 11.43m, respectively). Similarly, the mean differences from *Ha* show the same tendency as that smaller absolute values for PRN 13 and 5 (0.27, 0.50 m) and larger absolute values for PRN 28, 30 and 44 (-2.50, 3.88, -3.17 m). The accuracy of these *h* estimation for each GPS satellite is significantly related with their elevation angles (Table 1), except for PRN 44; estimations become more accurate when the elevation angles of GPS satellites are high. This relationship, however, does not fit to PRN 44 since the elevation angles of PRN 44 (approximately 44.4°) is slightly larger than that of PRN 5 (approximately 42.8°).

Table 2. *Statistics of the Difference between the Measured and Estimated Heights*

Original estimation by Eq. (2)					
PRN	13+5+28+30+44				
Mean diff. [m]	-0.72				
RMS diff. [m]	5.87				
Individual GPS estimates in Eq. (3)					
PRN	13	28	30	5	44
Mean diff. [m]	0.27	-2.50	3.88	0.50	-3.17
RMS diff. [m]	3.30	17.07	26.80	3.82	11.43
Least square methods in Eq. (4)					
PRN	13+5	13+5+28+30		13+5+28+30+44	
Mean diff. [m]	0.36	0.35		-0.51	
RMS diff. [m]	3.37	3.74		4.12	

Among three GPS satellites with less accurate estimations, high-frequency variations with approximately five-second periods are present during the whole duration in PRN 28 (Fig. 4c) and PRN 30 (Fig. 4d), although they tend to be suppressed at around 29.5 min. Meanwhile, for PRN 44, these high-frequency variations are less significant but extremely large spiky outliers are occasionally recorded, i.e. at around 27.75 min and 28.6 min. This would suggest, as anticipated, that errors from local sources, such as lands, are contaminated only in PRN 44, which also explains why the estimation accuracy is low in spite of the relatively high elevation angles.

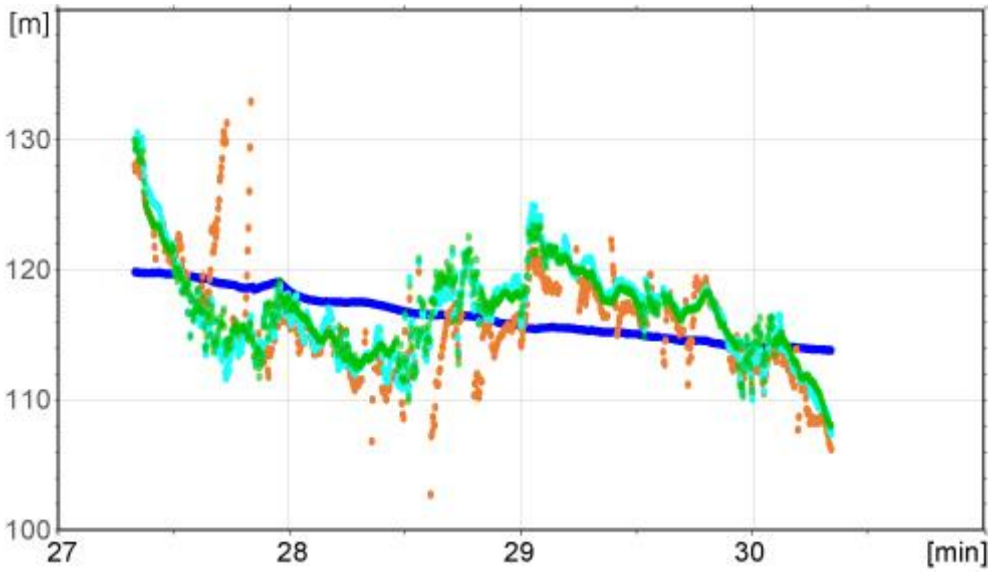

Figure 5. Time series of the estimated height *h* by the least square method in Eq. (4) from data of five GPS satellites (orange), four GPS satellites excluding PRN 44 (magenta) and two GPS satellites PRN 13 and 5 (green). The measured height *Ha* is also plotted by blue dots.

Applying the least square method in Eq (4), the estimated height after the removal of ΔT^e is determined (Fig. 5). The estimation with all five GPS satellites results in the better accuracy than the original estimation, both in the mean and RMS differences (Table 2). When the data of PRN 44 that could be contaminated by lands are excluded, the accuracy becomes better. The mean difference from the measured height *Ha* is 0.35 m, and the RMS difference is also reduced from 5.87 m to 3.74 m. Meanwhile, the mean and RMS differences do not change much when data from low-elevation-angle GPS satellites (PRN 28 and 30) are further excluded, suggesting that they contribute less to the estimation in Eq. (4). .

4 Discussion and Summary

As seen in Fig. 5, the recursive constraint of temporal continuity of ΔT certainly suppress high-frequency noises seen in the original *h* estimation (Fig. 4a). However, there still exist long-term variations with periods exceeding one minute with an amplitude of approximately 5 m. Since simple quadratic function ΔT^e was applied to the noisy ΔT in the present study, more complicated functions could be adopted that allow few-minute variations of clock accuracy of the receivers. Note that, however, extensively complex functions may not be meaningful since the estimate of ΔT itself has already been heavily contaminated by the use of GNSS satellites with low elevation angles or possible land reflections. The best functional forms for extracting unknown true ΔT from noisy observations would be discussed in future studies. Remind that ΔT^e in the present study is estimated from a large number of individual ΔT estimates, so that the practical number of GNSS observations concerning with a single-epoch estimation of h in Eq. (4) is consequently increased than the original estimation in Eq. (2).

Figure 4 and Table 2 indicate that errors in the *h* estimations are sensitive both to the elevation angles and unexpected reflections such as ones from lands or ships. The former errors may not be critical since their contribution to the *h* estimation is less if GNSS satellites

with higher elevation angles are available. Meanwhile, unexpected reflections may not negligible as in Fig. 4. Since low-const GNSS-R altimeters are supposed to be used in coastal seas and lakes or ponds where numbers of natural or artificial structures are present, careful treatments on unexpected reflections other than water surface are necessary.

The present method has improved the GNSS-R measurement accuracy from 0.72 m to 0.35 m, although which would still not be enough for some researches. However, note that the present study treats the worst case when the altitude of the UAV is high and the number of available GNSS satellites is small. Easily, the hovering altitude of a UAV can be set lower. Remind also that a lower altitude will confirm that GNSS-R reflection points will be not far away from the nadir so that unexpected reflections from ships and lands are less likely included. The number of satellites can be increased by including other GNSS satellites such as BeiDou, GLONASS and QZSS. Following these suggestions, experimental observations with multi-types GNSS satellites at lower hovering altitudes will be reported in separated papers.

Acknowledgments

This study was discussed at the 2019 Pacific-Asian Marginal Seas (PAMS) Meeting. We thank Dr. Masanori Konda at Kyoto University and Mr. Kei Yufu at Kyushu University for their collaborations in conducting observations and deployment of the sensors on the UAV, respectively. All data used in the present study are attached as a supplemental data file. This work was partially supported by the Collaborative Research Program of Research Institute for Applied Mechanics, Kyushu University, and JSPS KAKENHI Grant Number JP20H05168.

References

Cretaux, J.-F., Calmant, S., Romanovski, V., Perosanz, F., Tashbaeva, S., Bonnefond, P., Moreira, D., Shum, C.K., Nino F., Berge-Nguyen, M., Fleury, S., Gegout P., Abarca del Rio, R. & Maisongrande, P. (2011), Absolute Calibration of Jason Radar Altimeters from GPS Kinematic Campaigns over Lake Issykkul. *Mar. Geod*., 34, 291-318, doi:10.1080/01490419.2011.585110

Fayad I., Baghdadi, N., Bailly, J.S., Frappart, F. & Zribi M. (2020), Analysis of GEDI elevation data accuracy for inland waterbodies altimetry. *Rem. Sens.*, 12(17), 2714. doi:10.3390/rs12172714

Fu, L.L. & Cazenave, A. (2001), *Satellite Altimetry and Earth Sciences: A Handbook of Techniques and Applications.* Academic Press, San Diego, CA, USA, 2001, 463pp, ISBN 0-12-269545-3

Fu, L.L., Alsdorf, D., Morrow, R. & Rodriguez, E. (2012), *SWOT: The Surface Water and Ocean Topography Mission*, available on line: https://swot.jpl.nasa.gov/system/documents/files/2179_2179_SWOT_MSD_1202012.pdf

Ichikawa, K., Ebinuma, T., Konda, M. & Yufu K. (2019), Low-cost GNSS-R altimetry on a UAV for water-level measurements at arbitrary times and locations. *Sensors*, 19, 998. doi:10.3390/s19050998

Ichikawa, K., Wang, X.F. & Tamura, H. (2020), Capability of Jason-2 subwaveform retrackers for significant wave height in the calm semi-enclosed Celebes Sea, *Rem. Sens.*, 12, 3367, doi:10.3390/rs12203367

Lin, Y.C., Cheng, Y.T., Zhou, T., Ravi, R., Hasheminasb, S.M., Flatt, J.E., Troy, C. & Habib, A. (2019), Evaluation of UAV LiDAR for Mapping Coastal Environments. *Rem. Sens.*, 11, 2893, doi:10.3390/rs11242893

Lowe, S.T., Zuffada, C., Chao, Y. Kroger, P., Young, L.E. & LaBrecque, J.L., 5-cm-Precision aircraft ocean altimetry using GPS reflections, *Geophys., Res. Lett.*, 29, 1375

Martin-Neira, M., Colmenarejo, P., Ruffini, G. & Serra C. (2002), Altimetry precision of 1 cm over a pond using the wide-lane carrier phase of GPS reflected signals, *Can. J. Rem. Sens.*, 28(3), 294-403

Passaro, M., Cipollini, P., Vignudeli, S., Quartly, G.D. & Snaith , H.M. (2014), ALES: A multi-mission adaptive subwaveform retracker for coastal and open ocean altimetry, *Rem. Sens. Environ.*, 145, 173-189, doi:10.1016/j.rse.2014.02.008

Roussel, N., Frappart, F., Ramillen, G., Darrozes, J., Desjardins, C., Gegout, P., Perosanz, F. & Biancale, R. (2014), Simulations of direct and reflected wave trajectories for ground-based GNSS-R experiments, *Geosci. Mod. Dev.*, 7, 2261-2279, doi:10.5194/gmd-7-2261-2014

RTKLIB: An Open Source Program Package for GNSS Positioning, Available on line: http://www.rtklib.com/ (accessed on 1 December 2018)

Ruffini, G., Soulat, F., Caparini, M., Germain, O. & Martin-Neira, M. (2004), The Eddy Experiment: Accurate GNSS-R ocean altimetry from low altitude aircraft, *Geophys. Res. Lett.*, 31, L12306, doi:10.1029/2004GL01994

Zlinszky, A., Boergens, E., Glira, P. & Pfeifer, N. (2017), Airborne Laser Scanning fro calibration and validation of inshore satellite altimetry: A proof of concept, *Rem. Sens. Environ.*, 197, 35-42, doi: 10.1016/j.rse.2017.04.027